



Article

Lightweight 3D-Printed Fractal Gradient-Index Lens Antenna with Stable Gain Performance

Yeonju Kim, Duc Anh Pham, Ratanak Phon and Sungjoon Lim *

School of Electrical and Electronics Engineering, Chung-Ang University, Seoul 06974, Korea

* Correspondence: sungjoon@cau.ac.kr; Tel.: +82-2-820-5827

Abstract: This paper proposes a millimeter-wave lens antenna using 3-dimensional (3D) printing technology to reduce weight and provide stable gain performance. The antenna consists of a four-layer cylindrical gradient-index (GRIN) lens fed by a wideband Yagi antenna. We designed a fractal cell geometry to achieve the desired effective permittivity for a GRIN lens. Among different candidates, the honeycomb structure is chosen to provide high mechanical strength with light weight, low dielectric loss, and lens dispersion for a lens antenna. Therefore, the measured peak gain was relatively flat at 16.86 ± 0.5 dBi within 25–31.5 GHz, corresponding to 1 dB gain bandwidth = 23%. The proposed 3D-printed GRIN lens is cost-effective, with rapid and easy manufacturing.

Keywords: lens antenna; millimeter-wave antenna; Yagi-Uda antenna; three-dimensional printing; fractal unit cell



Citation: Kim, Y.; Pham, D.A.; Phon, R.; Lim, S. Lightweight 3D-Printed Fractal Gradient-Index Lens Antenna with Stable Gain Performance. *Fractal Fract.* **2022**, *6*, 551. <https://doi.org/10.3390/fractalfract6100551>

Academic Editors: Peter Z. Petkov and Carlo Cattani

Received: 22 August 2022

Accepted: 26 September 2022

Published: 29 September 2022

Publisher's Note: MDPI stays neutral with regard to jurisdictional claims in published maps and institutional affiliations.



Copyright: © 2022 by the authors. Licensee MDPI, Basel, Switzerland. This article is an open access article distributed under the terms and conditions of the Creative Commons Attribution (CC BY) license (<https://creativecommons.org/licenses/by/4.0/>).

1. Introduction

Fifth-generation (5G) wireless communication is a revolutionary technology providing high-data-rate communications, low latency, and massive connectivity required for various applications (e.g., mobile, autonomous vehicles, and Internet of Things) [1–5]. However, several challenges must be addressed to realize 5G wireless networks, including access bounds, bandwidth, performance, and latency limitations from earlier generation communication system. Therefore, the millimeter-wave (mm-wave) frequency spectrum (including 26, 28, and 39 GHz) has been explored to secure sufficient bandwidth and achieve higher data rate. These frequency spectrums allow wide bandwidth and hence enable high data rates to meet the increasing system capacity and superfast connectivity requirements [6–9]. Component performance in mm-wave frequency bands may be degraded due to high path loss and implementation challenges compared to lower frequency bands. Therefore, it is essential to develop cost-effective antennas with high gain, high radiation efficiency, and wide bandwidth in the mm-wave frequency bands to achieve high data transmission rates for 5G.

Lens antenna convergence and divergence properties convert the spherical wave radiated from the feed antenna into the in-phase plane wave at the lens surface. Many recent studies have investigated mm-wave antennas with lenses since the planar phase front of the lens can produce a focused radiation beam with high gain and narrow beamwidth [10]. Recent studies on lens antennas can be classified into homogeneous and inhomogeneous lens antenna. The former refers to the structure in which the media inside the lens are unchanged. For manipulating the electromagnetic (EM) wave propagation, these lens typically are designed with the convex or spherical interfaces. Due to this geometrical feature, the homogeneous lens antenna has to suffer with the disadvantage of bulky and non-planar structure. Instead of depending on the interfaces of lenses, the inhomogeneous lens antenna has flat structure that is typically constructed from several concentric layers of different materials with gradient refractive indexes to focus the EM energy toward the desired focusing direction. Because of its gradient refractive index profile, this type of lens is well-known as the gradient-index (GRIN) lens antenna. Compared to classic

homogeneous lens antennas, GRIN lens antennas can be compact and lightweight while maintaining high efficiency [11].

Recent studies on GRIN lens antennas have been separated based on the fabrication technology of printed-circuit-board (PCB) and three-dimensional (3-D) printing. Although PCB-based lens antennas have recently been well studied [12–15], the frequency increment into the millimeter-wave spectrum for broadening the bandwidth has put considerable pressure on the fabrication system for much higher accuracy. Therefore, complex manufacturing processes and high manufacturing costs are generally utilized in GRIN lens antenna fabrication. 3D printing technology creates 3D objects by depositing materials in successive layers and has been used to manufacture lens antennas due to the simple and cost-effective manufacturing process. A 3D-printed discrete dielectric lens was designed for high gain and beam scanning using a periodic and antireflection structure with the GRIN structure comprising stratified hemispherical shells [16,17]. A comb mushroom shaped dielectric lens achieved stable gain enhancement [18]. A circularly polarized lens antenna implemented by a 3D-printed dielectric polarizer was presented [19]. The Luneburg lens antenna composed of rod-type dielectric rings introduced multi-beam for MIMO applications in Ka-band [20].

Various configurations to realize the required lens permittivity distribution could be efficiently produced using 3D printing technology [21]. Many reported lens antennas have been manufactured using polyjet or SLA methods because they provide high-resolution output with very detailed and fine features [22,23]. However, methods using photopolymers increase manufacturing cost and require additional post-processing, such as manual support removal. On the other hand, fused deposition modelling (FDM) using a thermoplastic filament provides a simpler and cheaper process than the SLA. A GRIN lens antenna was fabricated using FDM with polylactic acid (PLA) as the 3D printing polymer [24] and obtained a maximum gain of 24 dBi with low cost and easy fabrication.

This paper proposes a lightweight GRIN lens antenna with stable gain performance in mm-wave frequency band using FDM 3D printing. The proposed high-gain lens antenna incorporated a hollow fractal structure and was fabricated with an easy-to-handle and cost-effective PLA filament. Though there are diverse fractal structures that are explored and utilized in designing antenna and metamaterial [25–27], the honeycomb structure is chosen for this design due to its unique features of being mechanically strong and light at the same time. Owing to this valuable feature, we can achieve a relatively low dielectric loss without reducing the mechanical strength of the total structure. Furthermore, the honeycomb structure has a simple topological structure that can easily be realized with low-cost 3D printers. We investigated how hollow honeycomb structure electrical properties depended on honeycomb cell sizes to realize the relative permittivity required for GRIN lens layers. The dielectric loss of 3D printing the polymer and overall lens antenna weight significantly reduced using the hollow honeycomb geometry. A wideband Yagi antenna was designed and combined with the honeycomb-shaped GRIN lens to examine the proposed lens antenna performance. Antenna characteristics, including return loss and radiation performance, were verified numerically and experimentally.

2. 3D-Printed Lens and Source Antenna Design

2.1. 3D-Printed Fractal GRIN Lens Design with Honeycomb Cells

Figure 1 shows an inhomogeneous cylindrical GRIN lens, which is a gradient refractive index lens with different relative permittivity ϵ_r for each layer. For designing the GRIN lens antenna, the diameter D_{lens} and focal distance D_f need to be firstly chosen. The gradient-index profiles for designing the GRIN lens antenna then can be achieved by controlling the relative permittivity of each concentric layer following this equation [28]:

$$\epsilon_n = \left(\frac{D_1 - D_n + \sqrt{\epsilon_1} t_{\text{lens}}}{t_{\text{lens}}} \right)^2 \quad (1)$$

where $n = 1, 2, 3, \dots, N$ is the number of concentric layers, ϵ_n is the permittivity of the concentric layer n^{th} and D_n is the distance from the focusing point to the respective concentric

layers. Because ϵ_1 respects to the first concentric layer in the center, ϵ_1 should have the highest value and is secondly chosen [24]. After that, the relative permittivity of other concentric layers can be sequentially calculated. However, it is difficult to realize the continuous permittivity variation for an ideal GRIN lens in practice due to technical constraints. Thus, a GRIN lens is generally designed in forms of a finite number of concentric homogeneous layers, as shown in Figure 1b, where the relative permittivity and radius for each layer obey Equation (1). It is worth noting that the higher the number of concentric layers that are used, the more similarity can be achieved between the theoretical continuous relative permittivity curve and the designed discretized relative permittivity [24]. However, it would increase the complexity of the design structure, and thus it requires higher accuracy fabrication systems. Meanwhile, GRIN lens antenna performance is also affected by the lens dimension. The lens antenna's aperture efficiency can decrease as the diameter of the lens increases. For those reasons, there is a trade-off between performance and ease of manufacturing when selecting the number of layers in the lens.

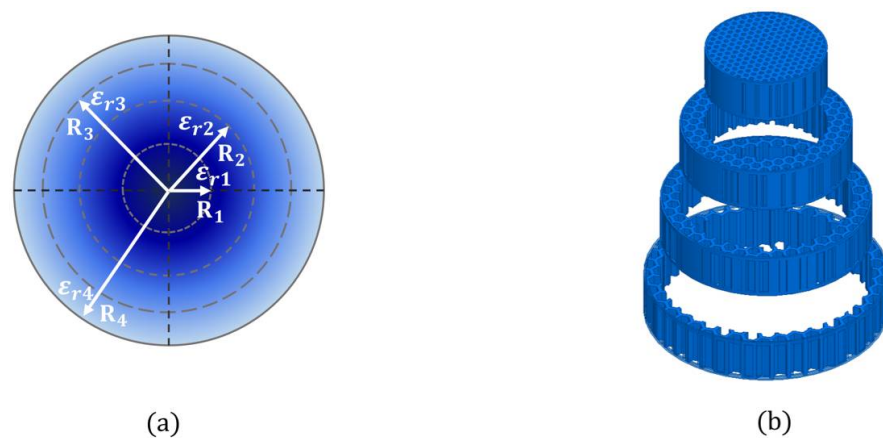


Figure 1. Proposed GRIN lens concept: (a) four-layer cylindrical GRIN lens, and (b) 3D-printed GRIN lens with honeycomb unit cells.

Considering these issues, we proposed the lens outer layer diameter be set as $6\lambda_0$, the focal distance as $8.87\lambda_0$, and the total number of layers = 4. Table 1 shows the relative permittivity and radius for the GRIN lens layers with the lens outer diameter = $6\lambda_0$ at 28 GHz. The relative permittivity and radius for each layer are 1.88–1.22, and 16.1–32.1 mm, respectively.

Table 1. Proposed GRIN lens design parameters.

Parameters	1	2	3	4
Permittivity	1.88	1.67	1.44	1.22
Radius (mm)	16.1	22.7	27.8	32.1

We used a honeycomb structure for the unit cells in each layer to realize layers with derived relative permittivity. The honeycomb structure is suitable for lens design, providing efficient unit cell deployment for continuous permittivity variation and mechanical stability and durability. Polylactic acid filament (dielectric constant of $\epsilon_r = 2.2$, dielectric loss of $\tan\delta = 0.05$) was used to 3D print the lens with the honeycomb structure. Effective permittivity for the honeycomb unit cell size was investigated by two methods of filling ratio method and transmission line method. Following the equation from the former technique, we can calculate the effective permittivity of the honeycomb cell based on the ratio of unfilled and filled portions in the cells [11], as shown in Equation (2). Meanwhile, the latter technique examines the S-parameters of structures that contain the honeycomb cells and uses the curve-fitting method to determine its effective permittivity [29]. Effective permittivity can

be derived from the following simple equation using the filling ratio of the 3D printing material [11].

$$\varepsilon_{re} = \varepsilon_r \frac{V_0 - V_i}{V_0} + \frac{V_i}{V_0} \quad (2)$$

where ε_r is the 3D-printed material permittivity, V_0 is the overall volume of the 3D-printed honeycomb cell filled with PLA, and V_i is the inner volume of 3D-printed honeycomb cell filled with air. For the transmission line method, we examined the scattering parameters within 24–32 GHz by electromagnetic (EM) simulation assuming that two different length dielectrics consisting of the honeycomb unit cells are inserted into the waveguide. EM simulations were performed using the ANSYS high-frequency structure simulator (HFSS). Figure 2 shows effective permittivity for the honeycomb unit cell with respect to the diagonal length (L_h). Honeycomb cell thickness (T_h) was fixed to 1 mm to reduce the filament dielectric loss and print easily. When the honeycomb cell diagonal length (L_h) increased from 1.25 to 4 mm, the effective permittivity obtained using the filling ratio method decreased from 1.81 to 1.23, whereas the effective permittivity obtained using the transmission line method decreased from 1.85 to 1.2.

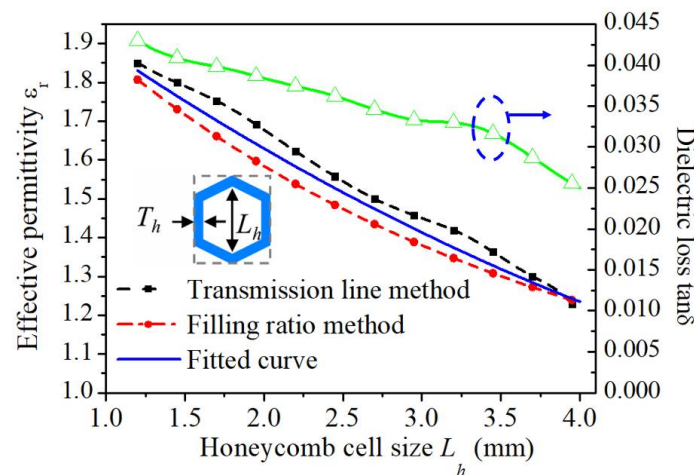


Figure 2. Effective permittivity (left axis) and dielectric loss (right axis) of honeycomb cell versus different size of honeycomb cells L_h .

The effective permittivity estimated from these two methods shows a slight difference since the honeycomb cell geometry is used in the filling ratio method, and the large area honeycomb-shaped dielectric is used in a specific frequency range for the transmission line method. The fitted curve for the honeycomb cell size effective permittivity was estimated as

$$\varepsilon_r = 0.019L_h^2 - 0.3119L_h + 2.1767 \quad (3)$$

using data from both methods, with the honeycomb cell size for each layer = 1.03, 1.85, 2.85, and 3.99 mm. The dielectric loss for each layer decreased from 0.045 to 0.025 when the honeycomb cell size increased from 1.03 to 3.99 mm, as indicated with the green line in Figure 2. It can be observed that the smaller the honeycomb cell size, the higher the permittivity that can be achieved. However, when the honeycomb cell size decreases, creating the unfilled area with higher accuracy is considerably challenging. In addition, decreasing the unfilled area also means increasing the weight of the designed GRIN lens. Due to this reason, different with other designs, the center concentric layer ($n = 1$) in the proposed GRIN lens has a much wider area and does not follow the gradient rule. Although there will be a slight trade-off with the radiation gain, the weight and fabrication complexity can be considerably reduced.

2.2. Source Antenna Design

To remain a light weight and compact structure while still satisfying the conditions of high gain, high directivity, and wideband, the Yagi antenna was chosen as the source antenna for verifying the performance of the proposed 3D-printed GRIN lens. Yagi antennas are suitable to integrate with a honeycomb-shaped GRIN lens because they provide wide bandwidth and end-fire radiation with compact size [30]. Figure 3 shows the top and bottom geometry of the Yagi antenna. The antenna was designed on a Duroid RT5880 substrate ($\epsilon_r = 2.2$, $\tan\delta = 0.0009$) with a thickness of 0.51 mm. Nine directors with length $L_d = 2.5$ mm and width $W_d = 0.6$ mm were used to achieve high gain. Different L_1 and L_2 were used on the top and bottom of the Yagi antenna for impedance matching. Due to its polarization characteristic, the E-plane and H-plane of the designed Yagi antenna are the YZ and XZ planes, respectively. The simulated half-power beamwidth (HPBW) was 45.6° and 54.5° in the E-plane and H-plane, respectively, at 28 GHz, as shown in Figure 4a. The simulated peak gain of Yagi antenna was 6.8–11.4 dBi for 24–32 GHz. The simulated fractional impedance bandwidth of the Yagi antenna was found to be 35.7%. The Yagi antenna was designed with sufficient bandwidth and gain to validate the proposed fractal GRIN lens in the mm-wave frequency band.

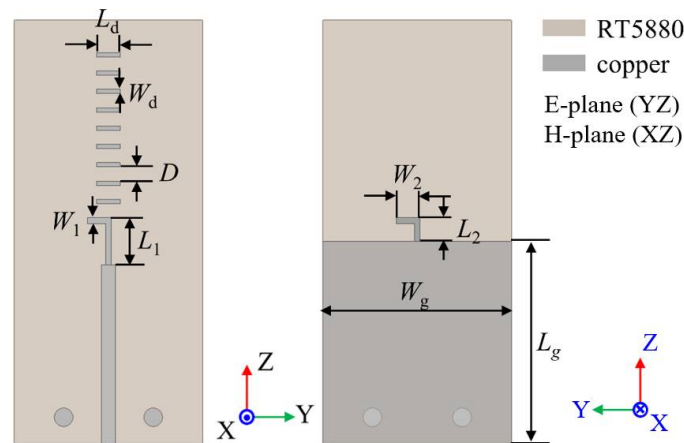


Figure 3. Yagi antenna geometry with design parameters (units: mm): $W_g = 20$, $L_g = 22$, $W_1 = 0.6$, $L_1 = 5$, $L_3 = 2.5$, $L_2 = 2.5$, $W_d = 0.6$, $L_d = 2.5$, $D = 1.2$.

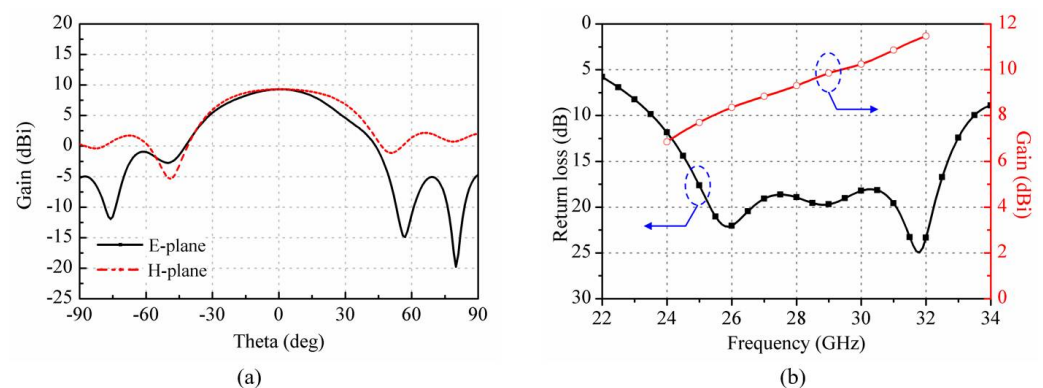


Figure 4. Simulated Yagi antenna parameters: (a) radiation pattern at 28 GHz, and (b) return loss (left axis) and gain (right axis).

2.3. Source Antenna Integrated with Fractal GRIN Lens Using Honeycomb Cells

Figure 5 demonstrates the proposed honeycomb-shaped GRIN lens fed by the Yagi antenna. The lens was designed by placing four honeycomb cells of different size in a circular cylinder made of PLA. The four layers comprised the hollow honeycomb cells with $L_{h1} = 1.03$ mm, $L_{h2} = 1.85$ mm, $L_{h3} = 2.85$ mm, $L_{h4} = 3.99$ mm to realize the de-

sired relative permittivity of the lens. Each layer was connected by a 0.5 mm thick ring (Figure 5b, dashed line) inserted on the top and bottom of the layers.

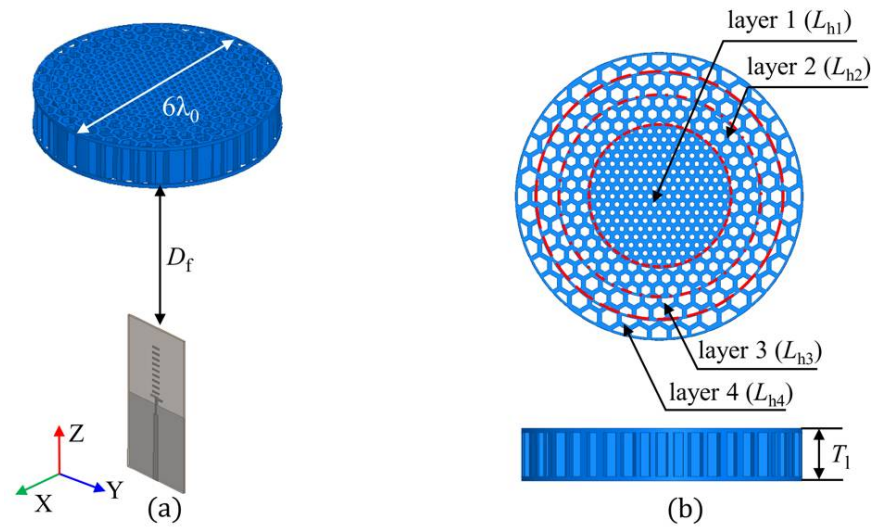


Figure 5. (a) Source antenna integrated with GRIN lens; (b) fractal GRIN lens with honeycomb cells top and side view.

The source antenna was aligned with the center of the lens in the x - y plane and D_f from the lens in the z plane. Focal length D_f between source antenna and lens was investigated by simulation to achieve optimal gain and minimal sidelobe levels (SLL) while retaining wide bandwidth. Figure 6a,b show that the antenna gain and the sidelobe level depend on the lens thickness T_1 and the lens focal length D_f after loading the honeycomb-shaped GRIN lens. As T_1 increased from 5 to 20 mm, the antenna gain enhanced from 13.1 to 19.1 dBi. The sidelobe level of the antenna decreased from -9.7 to -14.5 and from -8.6 to -13.5 dB for the E-plane and H-plane, respectively.

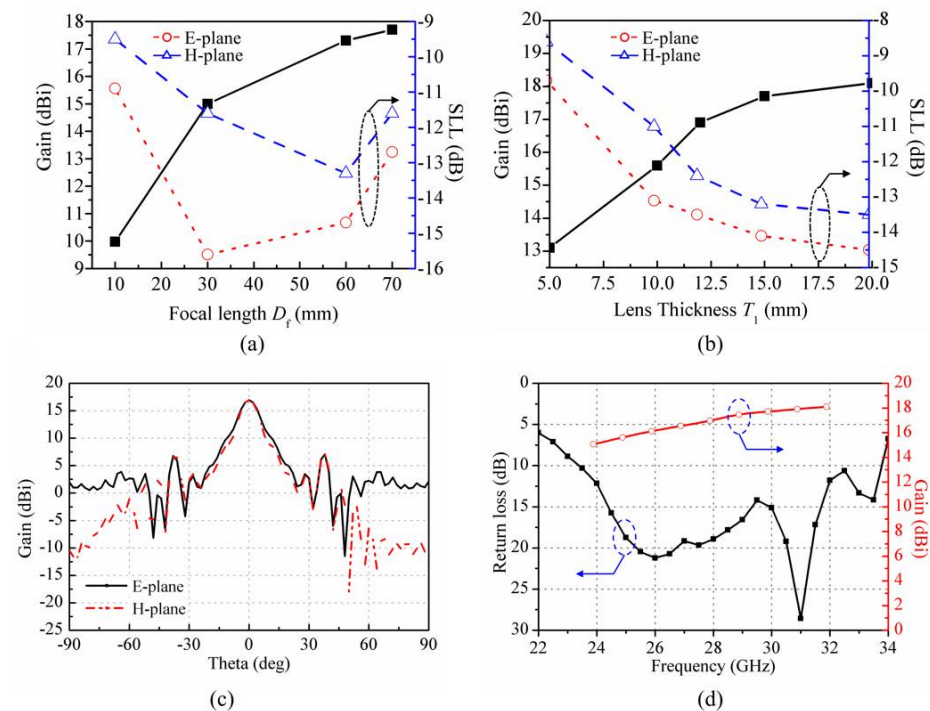


Figure 6. Simulated gain (left axis) and sidelobe level (right axis) of proposed structure at 28 GHz versus (a) focal length D_f , and (b) lens thickness T_1 ; (c) Simulated 2D radiation patterns of proposed structure at 28 GHz; and (d) return loss (left axis) and gain (right axis).

A thicker lens will improve the lens focusing ability, increasing gain and reducing sidelobe level. However, the antenna efficiency degrades due to the dielectric loss from PLA. Thus, the lens thickness was set to 12 mm. Figure 6a shows the antenna gain and sidelobe level with respect to the focal length when the lens thickness was 12 mm. The antenna gain increased from 9.98 to 17.7 dBi as the focal length increased from 10 to 70 mm, and the optimal sidelobe level occurred at -14.7 dB and -13.3 dB for the E-plane and H-plane, respectively, for the lens focal length = 60 mm. The lens antenna gain and sidelobe level are significantly affected by the phase distribution at the lens surface, and the phase distribution depends on the focal length. Therefore, although the structure was initially calculated with the focal length D_f of $8.87\lambda_0$, we set the focal length between the source antenna and the lens to 60 mm for optimizing both the higher antenna gain and lower sidelobe level.

Figure 6c,d shows the simulated radiation pattern, gain, and return loss when the honeycomb-shaped GRIN lens was fed by the Yagi antenna. The half-power beamwidth reduced from 42.6° to 10.8° and from 50.5° to 9.8° for the E-plane and H-plane, respectively, with the peak gain of 16.9 dBi at 28 GHz. The fractional impedance bandwidth for the Yagi antenna combined with the honeycomb-shaped GRIN lens was 36.8%. The antenna peak gain was from 15.57 to 18.09 dBi within 24–32 GHz. Thus, the Yagi antenna integrated with the proposed lens achieved high gain, narrow beamwidth, and wide bandwidth with the optimized lens focal length and thickness.

3. Experimental Investigation and Discussion

Figure 7a shows the fabricated proposed honeycomb-shaped GRIN lens using 3D printing technology, to demonstrate the proposed concept. A commercial desktop 3D printer (Sindoh 3DWOX 2X) using fused filament fabrication was used to print the honeycomb-shaped GRIN lens. The diameter of the 3D printer filament extrusion nozzle was 0.4 mm, and the layer resolution was provided from 0.05 to 0.4 mm. For the prototype fabrication, we set the layer resolution = 0.2 mm, the printing speed = 60 mm/s and the nozzle moving speed = 100 mm/s. Due to the simple printing conditions for the PLA filament, the lenses can be easily and rapidly manufactured at low cost. The Yagi antenna was fabricated by conventional PCB processing with the RT5880 substrate. We combined the honeycomb-shaped GRIN lens and Yagi antenna with a 3D-printed PLA supporting structure to ensure alignment. Figure 7b shows the simulated and measured return loss for a Yagi antenna and the Yagi antenna with honeycomb-shaped GRIN lens. The return loss for the fabricated sample was measured using a Keysight N5227B. The simulated and measured fractional impedance bandwidth for the Yagi antenna was 35.7% and 41.8%, respectively; by contrast, the simulated and measured fractional impedance bandwidth for the Yagi antenna integrated with the honeycomb-shaped GRIN lens was 36.7% and 40.7%, respectively. The simulated and measured return loss shows good agreement, and the proposed lens antenna provided sufficient operating bandwidth in mm-wave frequency band including 28 GHz.

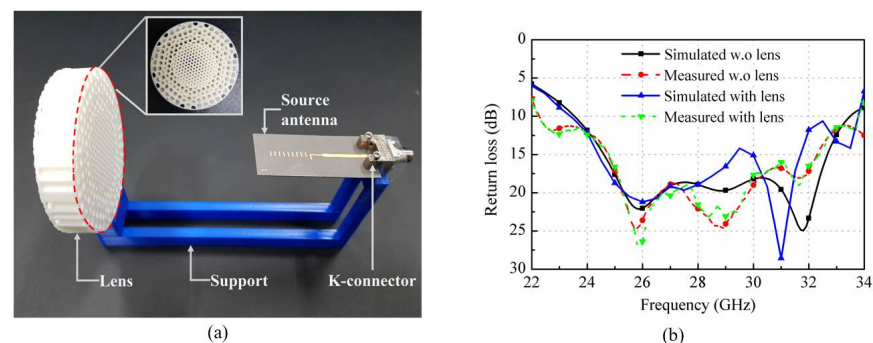


Figure 7. (a) Fabricated prototype fractal GRIN lens using honeycomb cells fed by Yagi antenna. (b) Simulated and measured return loss for Yagi antenna and Yagi antenna with proposed fractal GRIN lens.

Figure 8a shows the setup to measure the radiation performance for the fabricated sample using a commercial ORBIT/FR far-field measurement system in a shielded millimeter-wave anechoic chamber room. The standard gain horn antenna HO42S was used for the frequency range from 24–26.5 GHz, and HO28S was used for the frequency range from 26.5–32 GHz [7]. Figure 8b,c compare the measured and simulated Yagi antenna radiation pattern at 28 GHz. The measured peak gain was 9.03 dBi, and the measured HPBW was 41.6° and 51.38° in the E and H-plane, respectively.

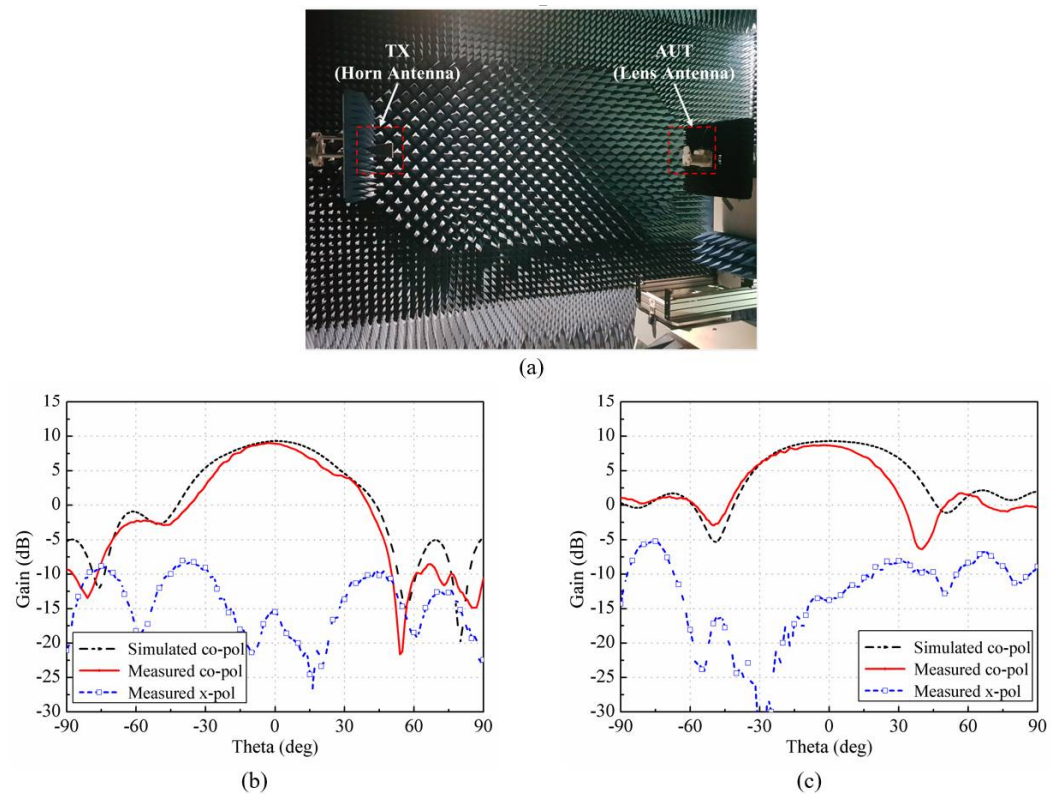


Figure 8. (a) Far-field radiation pattern measurement setup; simulated and measured radiation pattern for Yagi antenna at 28 GHz in (b) E-plane and (c) H-plane.

Figure 9 shows simulated and measured radiation patterns for the combined Yagi antenna and the fractal GRIN lens using the honeycomb cells on the E and H-planes. The measured peak gain for the proposed honeycomb-shaped GRIN lens antenna was 15.49, 16.86, and 17.66 dBi at 24, 28, and 32 GHz. The cross-polarization level was 26.5, 20.5, and 18.2 dB at 24, 28, and 32 GHz. The sidelobe level was -14.7 and -13.9 dB for the E and H-plane at 28 GHz, respectively. Figure 10 shows that the measured peak gain increased 7.5–8.84 dB over 24–32 GHz. The measured peak gain was relatively flat at approximately 16.86 ± 0.5 dBi within 25–31.5 GHz, corresponding to 1-dB gain bandwidth of 23%. The HPBW decreased to 9.87° – 11.68° and 8.07° – 10.79° in the E and H-plane for 24–32 GHz. The proposed lens antenna achieved radiation efficiency of 85.6–92.5% for 24–32 GHz, as indicated by the purple line in Figure 10. The hollow honeycomb structure reduced the dielectric loss from the 3D printing material and the overall lens weight. Hence, the proposed antenna exhibits stable gain with high efficiency in the mm-wave frequency band 24–32 GHz.

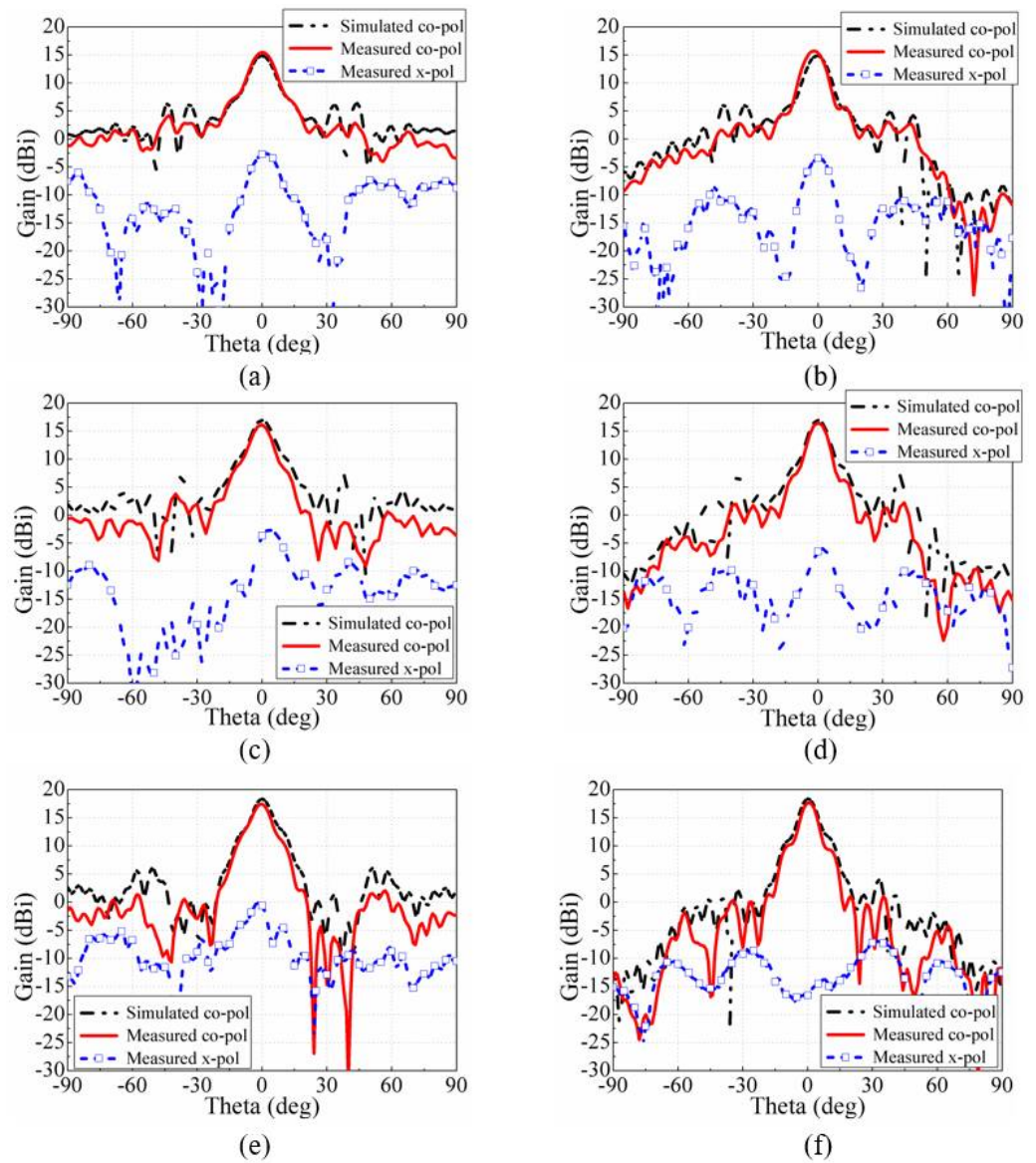


Figure 9. Simulated and measured radiation pattern for Yagi antenna with the proposed fractal GRIN lens in (a) E-plane and (b) H-plane at 24 GHz; (c) E-plane and (d) H-plane at 28 GHz; and (e) E-plane, and (f) H- plane at 32 GHz.

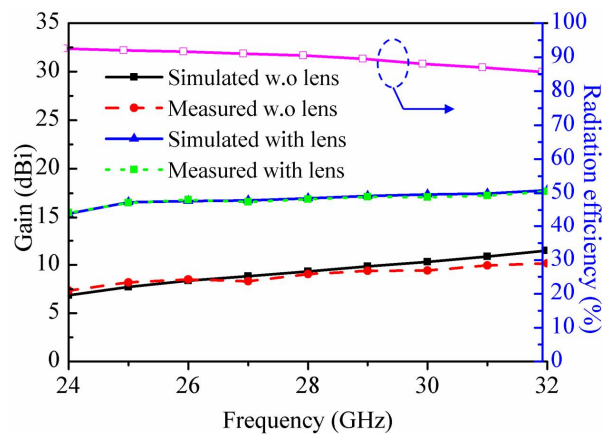


Figure 10. Simulated/measured gain (left axis) of Yagi antenna with/without proposed fractal GRIN lens and radiation efficiency (right axis) of final structure.

Table 2 compares the proposed lens antenna and other GRIN lens antennas. High-gain lens antennas with wide bandwidth in the mm-wave band using GRIN lenses have been reported previously [12–15]. However, the antennas required complicated manufacturing processes such as PCB and metal machining. GRIN lens antennas fabricated using 3D printing technology have also been presented previously [23,24,28]. However, the lens antennas used a high-end 3D printer due to the complicate lens unit structure required for elaborate fabrication. In contrast, the proposed fractal GRIN lens antenna is constructed from honeycomb cells produced by inexpensive FDM 3D printing using the PLA filament. Therefore, the proposed honeycomb-shaped GRIN lens provides a simple and cost-effective manufacturing process compared to the previous reported lenses. On the other hand, compared with other reported GRIN lens antenna, the proposed structure provides a widest 1-dB gain BW of 23%, the highest radiation efficiency of 92%, and a relatively wide impedance BW while remaining a simple and light weight overall structure.

Table 2. Comparison of proposed fractal GRIN lens antenna and other millimeter-wave lens antenna.

	[28]	[24]	[15]	[23]	This work
Source Antenna	Horn antenna	Patch antenna	Patch antenna	WG	Yagi
Lens volume ($W \times L \times H$) (mm)	$6\lambda_0 \times 6\lambda_0 \times 0.925\lambda_0$	$6.7\lambda_0 \times 6.7\lambda_0 \times 2.2\lambda_0$	$5\lambda_0 \times 5\lambda_0 \times 1.1\lambda_0$	$10\lambda_0 \times 10\lambda_0 \times 1.25\lambda_0$	$6\lambda_0 \times 6\lambda_0 \times 1.12\lambda_0$
Frequency band (GHz)	12–18	24–28	13.4–13.6	28–40	24–32
1dB gain BW (%)	N/A	<7.7	<4.7	<8% *	23
Impedance bandwidth (%)	N/A	15.4	1.48	42.4	41
SLL (dB)	−14 *	−11	−18.5	20 *	−17
Radiation Efficiency (%)	N/A	84.5	67.3	N/A	92
Lens material	PLA	Plastic resin	RO4350B	ABS1200, ABS1000, ABS650, ABS440, ABS300	PLA
Fabrication method	FDM	SLA	PCB	FDM	FDM
Cost	Low	High	Medium	High	Low
Weight	Light	Medium	Medium	Light	Very Light

* The data are estimated from the figure.

4. Conclusions

This paper proposed a 3D-printed fractal GRIN lens antenna with stable gain for mm-wave frequency band applications. The fractal GRIN lens was realized with different sized hollow honeycomb cells printed by a cost-effective FDM 3D printer. The proposed lens antenna exhibited relatively flat gain 16.86 ± 0.5 dBi due to the decreased dielectric loss in the 3D printing material from the hollow honeycomb structure. In addition, owing to the structure of the proposed GRIN lens with only four concentric layers and a relatively wide center concentric layer, the weight of the proposed GRIN lens antenna is significantly reduced, although there is a slight trade-off in the maximum radiation gain. The fabricated prototype lens has the weight of only 23 g while maintaining high mechanical strength. In addition, the proposed fractal GRIN lens antenna provides easy fabrication and low cost using commercial 3D printing technology. The proposed concept was successfully demonstrated and could be extended into a beam-reconfigurable lens antenna with high gain, wide bandwidth, and lightweight by introducing flexible or smart material to achieve a reconfigurable physical structure.

Author Contributions: Y.K. and S.L. conceived the idea. Y.K. designed, simulated, and experimentally verified the proposed concept and proposed designs. Y.K., D.A.P. and R.P. contributed to the fabrication and experiment processes. S.L. directed and supervised the project. All authors have contributed to writing the manuscript. All authors have read and agreed to the published version of the manuscript.

Funding: This work was supported by the National Research Foundation of Korea (NRF) grant funded by the Korea government (MSIT) (2021R1A4A2001316).

Data Availability Statement: Not applicable.

Acknowledgments: The authors would like to acknowledge the funding from the National Research Foundation of Korea (NRF) grant funded by the Korea government (MSIT), under the Grant No. 2021R1A4A2001316.

Conflicts of Interest: The authors declare no conflict of interest.

References

- Vallappil, A.K.; Khawaja, B.A.; Rahim, M.K.A.; Iqbal, M.N.; Chattha, H.T.; Ali, M.F. bin M. A compact triple-band UWB inverted triangular antenna with dual-notch band characteristics using SSRR metamaterial structure for use in next-generation wireless systems. *Fractal Fract.* **2022**, *6*, 422. [[CrossRef](#)]
- Tubbal, F.; Matekovits, L.; Raad, R. Antenna designs for 5G/IoT and space applications. *Electronics* **2022**, *11*, 2484. [[CrossRef](#)]
- Paun, M.-A.; Nichita, M.-V.; Paun, V.-A.; Paun, V.-P. Minkowski's loop fractal antenna dedicated to sixth generation (6G) communication. *Fractal Fract.* **2022**, *6*, 402. [[CrossRef](#)]
- Lee, J.-G. Compact and robust Fabry-perot cavity antenna with PEC wall. *J. Electromagn. Eng. Sci.* **2021**, *21*, 184–188. [[CrossRef](#)]
- Lim, J.-H.; Lee, J.W.; Lee, T.-K.; Ryu, S.-B.; Lee, H.-C.; Lee, S.-G. Optimal design of the reflector antenna to improve performance of C-band quad-pol ScanSAR systems. *J. Electromagn. Eng. Sci.* **2020**, *20*, 155–157. [[CrossRef](#)]
- Pham, D.A.; Park, E.; Lee, H.L.; Lim, S. High gain and wideband metasurfaced magnetoelectric antenna for WiGig applications. *IEEE Trans. Antennas Propag.* **2021**, *69*, 1140–1145. [[CrossRef](#)]
- Pham, D.A.; Lee, M.; Lim, S. High-gain conical-beam planar antenna for millimeter-wave drone applications. *IEEE Trans. Antennas Propag.* **2021**, *69*, 6959–6964. [[CrossRef](#)]
- Sarkar, A.; Pham, D.A.; Lim, S. 60 GHz Electronically tunable leaky-wave antenna based on annular surface plasmon polariton media for continuous azimuth scanning. *IEEE Trans. Antennas Propag.* **2022**. [[CrossRef](#)]
- Sarkar, A.; Pham, D.A.; Lim, S. Tunable higher order mode-based dual-beam CRLH microstrip leaky-wave antenna for V-band backward-broadside-forward radiation coverage. *IEEE Trans. Antennas Propag.* **2020**, *68*, 6912–6922. [[CrossRef](#)]
- Zhang, Y.S.; Hong, W. A millimeter-wave gain enhanced multi-beam antenna based on a coplanar cylindrical dielectric lens. *IEEE Trans. Antennas Propag.* **2012**, *60*, 3485–3488. [[CrossRef](#)]
- Liang, M.; Ng, W.-R.; Chang, K.; Gbele, K.; Gehm, M.E.; Xin, H. A 3-D Luneburg lens antenna fabricated by polymer jetting rapid prototyping. *IEEE Trans. Antennas Propag.* **2014**, *62*, 1799–1807.
- Su, Y.; Chen, Z.N. A flat dual-polarized transformation-optics beams scanning Luneburg lens antenna using PCB-stacked gradient index metamaterials. *IEEE Trans. Antennas Propag.* **2018**, *66*, 5088–5097. [[CrossRef](#)]
- Erfani, E.; Niroo-Jazi, M.; Tatu, S. A high-gain broadband gradient refractive index metasurface lens antenna. *IEEE Trans. Antennas Propag.* **2016**, *64*, 1968–1973. [[CrossRef](#)]
- Pfeiffer, C.; Grbic, A. Planar lens antennas of subwavelength thickness: Collimating leaky-waves with metasurfaces. *IEEE Trans. Antennas Propag.* **2015**, *63*, 3248–3253. [[CrossRef](#)]
- Papathanasopoulos, A.; Rahmat-Samii, Y.; Garcia, N.C.; Chisum, J.D. A novel collapsible flat-layered metamaterial gradient-refractive-index lens antenna. *IEEE Trans. Antennas Propag.* **2020**, *68*, 1312–1321. [[CrossRef](#)]
- Yi, H.; Qu, S.-W.; Ng, K.-B.; Chan, C.H.; Bai, X. 3-D printed millimeter-wave and terahertz lenses with fixed and frequency scanned beam. *IEEE Trans. Antennas Propag.* **2016**, *64*, 442–449. [[CrossRef](#)]
- Qu, Z.; Qu, S.-W.; Zhang, Z.; Yang, S.; Chan, C.H. Wide-angle scanning lens fed by small-scale antenna array for 5G in millimeter-wave band. *IEEE Trans. Antennas Propag.* **2020**, *68*, 3635–3643.
- Zhang, Y.-X.; Jiao, Y.-C.; Liu, S.-B. 3-D-printed comb mushroom-like dielectric lens for stable gain enhancement of printed log-periodic dipole array. *IEEE Antennas Wirel. Propag. Lett.* **2018**, *17*, 2099–2103.
- Wang, K.X.; Wong, H. Design of a wideband circularly polarized millimeter-wave antenna with an extended Hemispherical lens. *IEEE Trans. Antennas Propag.* **2018**, *66*, 4303–4308. [[CrossRef](#)]
- Li, Y.; Ge, L.; Chen, M.; Zhang, Z.; Li, Z.; Wang, J. Multibeam 3-D-printed Luneburg lens fed by magnetoelectric dipole antennas for millimeter-wave MIMO applications. *IEEE Trans. Antennas Propag.* **2019**, *67*, 2923–2933.
- Goulas, A.; Zhang, S.; McGhee, J.R.; Cadman, D.A.; Whittow, W.G.; Vardaxoglou, J.C.; Engström, D.S. Fused filament fabrication of functionally graded polymer composites with variable relative permittivity for microwave devices. *Mater. Des.* **2020**, *193*, 108871.
- Kim, Y.; Cui, Y.; Tentzeris, M.M.; Lim, S. Additively manufactured electromagnetic based planar pressure sensor using substrate integrated waveguide technology. *Addit. Manuf.* **2020**, *34*, 101225.
- Poyanco, J.-M.; Pizarro, F.; Rajo-Iglesias, E. Cost-effective wideband dielectric planar lens antenna for millimeter wave applications. *Sci. Rep.* **2022**, *12*, 4204. [[CrossRef](#)]
- Garcia-Marin, E.; Filipovic, D.S.; Masa-Campos, J.L.; Sanchez-Olivares, P. Low-cost lens antenna for 5G multi-beam communication. *Microw. Opt. Technol. Lett.* **2020**, *62*, 3611–3622. [[CrossRef](#)]

25. Werner, D.H.; Haupt, R.L.; Werner, P.L. Fractal antenna engineering: The theory and design of fractal antenna arrays. *IEEE Antennas Propag Mag.* **1999**, *41*, 37–58.
26. Ghaffar, F.A.; Khalid, M.U.; Salama, K.N.; Shamim, A. 24-GHz LTCC fractal antenna array SoP with integrated Fresnel lens. *IEEE Antennas Wireless Propag Lett.* **2011**, *10*, 705–708. [[CrossRef](#)]
27. Shookooh, B.R.; Monajati, A.; Khodabakhshi, H. Theory, design, and implementation of a new family of ultra-wideband metamaterial microstrip array antennas based on fractal and fibonacci geometric patterns. *J. Electromagn. Eng. Sci.* **2020**, *20*, 53–63. [[CrossRef](#)]
28. Zhang, S.; Arya, R.; Pandey, S.; Vardaxoglou, J.C.; Whittow, W.; Mittra, R. 3D-printed planar graded index lenses. *IET Microw. Antennas Propag.* **2016**, *10*, 1411–1419.
29. Janezic, M.D.; Jargon, J.A. Complex permittivity determination from propagation constant measurements. *IEEE Microw. Guided Wave Lett.* **1999**, *9*, 76–78. [[CrossRef](#)]
30. Alhalabi, R.A.; Rebeiz, G.M. High-gain Yagi-Uda antennas for millimeter-wave switched-beam systems. *IEEE Trans. Antennas Propag.* **2009**, *57*, 3672–3676.